Environmental Technology

ISSN: 0959-3330 (Print) 1479-487X (Online) Journal homepage: http://www.tandfonline.com/loi/tent20

Fixed-bed study for bone char adsorptive removal of refractory organics from electrodialysis concentrate produced by petroleum refinery

Patrícia da Luz Mesquita, Cássia Ribeiro Souza, Nilza Tatiane G. Santos & Sônia Denise Ferreira Rocha

To cite this article: Patrícia da Luz Mesquita, Cássia Ribeiro Souza, Nilza Tatiane G. Santos & Sônia Denise Ferreira Rocha (2018) Fixed-bed study for bone char adsorptive removal of refractory organics from electrodialysis concentrate produced by petroleum refinery, Environmental Technology, 39:12, 1544-1556, DOI: 10.1080/09593330.2017.1332691

To link to this article: https://doi.org/10.1080/09593330.2017.1332691

Accepted author version posted online: 17 May 2017.
Published online: 05 Jun 2017.

ENVIRONMENTAL TECHNOLOGY, 2018
VOL. 39, NO. 12, 1544–1556
https://doi.org/10.1080/09593330.2017.1332691

Taylor & Francis
Taylor & Francis Group

Fixed-bed study for bone char adsorptive removal of refractory organics from electrodialysis concentrate produced by petroleum refinery

Patrícia da Luz Mesquita[a,b], Cássia Ribeiro Souza[b], Nilza Tatiane G. Santos[b] and Sônia Denise Ferreira Rocha[a]

[a]Mining Engineering Department, Universidade Federal de Minas Gerais, Pampulha, Belo Horizonte, Brazil; [b]Chemical Engineering Department, Universidade Federal de São João del-Rei – Campus Alto Paraopeba, Fazenda do Cadete, Ouro Branco, MG, Brazil

ABSTRACT

Water reuse in industrial processes has been an increasing need encouraged in recent years. However, as the streams are recycled, solutes accumulate, thus requiring purification techniques. Membrane processes (reverse osmosis and electrodialysis) have been implemented and in order to increase the reuse of water at its highest level, crystallization has been evaluated to remove salts from the concentrate produced and get a feasible disposal. Nevertheless, contaminants affect the crystallization performance, thus making the removal of residual organics important for both the efficiency of crystallization and the increase of water reuse. In this context, aiming at establishing a sustainable virtuous circle, bone char (0.5–1.4 mm particle size, mesoporous structure) was used to remove refractory organics from an electrodialysis concentrate effluent (C-EDR) from a Brazilian petroleum refinery, at a lab-scale, in a fixed-bed adsorption column. Bone char selectively and partially removed the refractory organics, a complex mixture of long-chain hydrocarbons, aromatic compounds, carboxylic acids, amines and amides. The maximum adsorption capacity increased with the increase in bed depth and reduction in flow rate. A maximum removal of 35.60 mg g^{-1} was achieved for the highest bed depth evaluated (12.9 cm). The breakthrough curves indicated that bone char could adsorb part of the organic compounds from the C-EDR. The scaling up was possible for the C/C_0 ratios of 0.55, 0.60 and 0.65, providing a service time at about 16 days for 45% removal efficiency for typical real operational conditions used in the refinery.

ARTICLE HISTORY
Received 21 November 2016
Accepted 16 May 2017

KEYWORDS
Water reuse; adsorption; bone char; residual organics; petroleum industry

1. Introduction

The improvement of consolidated technologies and the search for viable and low-cost alternative processes for water reuse in industry have been increasingly encouraged in a water scarcity scenario [1–3]. The petrochemical industry, one of the most relevant sectors in Brazil, requires, during the process of oil refining, an average of 246–340 l of water/day per barrel of crude oil. Additionally, a quantity of wastewater around 0.4–1.6 times the volume of oil processed is generated [4]. Due to this high water demand, reuse can significantly reduce the processing costs in oil refineries. Consequently, it is necessary to implement water management systems that include both water use rationalization and the choice of the best treatment system.

Nevertheless, water reuse requires advanced (tertiary) treatment such as adsorption onto activated carbon, advanced oxidation processes and membrane separation processes (e.g. reverse osmosis or electrodialysis), to remove dissolved organic or/and inorganic compounds [5–9]. Membrane processes bring many advantages [10] and a high-quality permeate for reuse is produced; however, as water recirculates, increasing salinity is inevitably observed in concentrate streams. Crystallization of salts is an option for destination of such brines, but it is affected by the presence of diverse contaminants, including low-solubility salts and organic compounds [11].

Refractory organics from petroleum processing are also of great concern because they may bring corrosion, toxicity and carcinogenicity to streams. Typical organic contaminants, such as long-chain hydrocarbons, aromatic compounds (such as benzene and phenolic ones), amines and amides, have been identified in the concentrate from electrodialysis [11,12].

In this context, adsorption, a consolidated process, is a potential technique to be included in these systems. Bhatnagar et al. [13], Hashemi [14] and Brunson and Sabatini [15], among other authors, highlight its usual low-cost, operational simplicity and low area demand, compared to other advanced wastewater treatment processes such as advanced oxidation processes and reverse

CONTACT Patrícia da Luz Mesquita patriciamesquita@ufsj.edu.br Chemical Engineering Department, Universidade Federal de São João del-Rei – Campus Alto Paraopeba, Fazenda do Cadete, Ouro Branco, 36420 000. MG, Brazil

osmosis. In particular, the adsorption process is suitable for removal of low-concentration or highly toxic contaminants that cannot be removed by the conventional biological treatment [16].

However, the organics removal by adsorption in charcoal has already been carried out, but with high cost and the performance was affected by increasing salinity. In this context, low-cost alternatives, such as adsorbents produced from wastes, are becoming more and more attractive. Among them, bone char may be highlighted for water/wastewater applications, being widely researched in this field [14,15,17–30].

Bone char (consisting of 70–90% of calcium phosphate, low amounts of calcium carbonate and only 10% in weight of carbon) differs from the conventional activated carbons (mainly constituted of C). It presents moderate specific surface area (around 120$m^2\ g^{-1}$), as well as carbonates from its preparation process, characteristics that make it singular for wastewater treatment applications and industrial demands of water reuse, including metals removal [14,15,22,28,29]. Bone char can also be promising to compose a sustainable cycle, as it is produced from a voluminous waste from tannery, food industry and cattle breeding. After its use and exhaustion in the adsorption process, it could be possible to reuse the apatite, precariously crystallized in the bone char, as a renewable and efficient phosphate fertilizer for deficient soils [18,31].

Studies for organic and inorganic compounds removal by bone char have been reported in the literature; however, most of them use synthetic aqueous solutions, especially for fluoride removal [14,15,23,25,31–39]. No previous investigation was found on the applications for removal of refractory organics in real concentrate streams from electrodialysis in the petroleum industry. Thus, this is the focus of the present work, which presents the use of bone char in the removal of organics from real electrodialysis concentrate in a continuous lab-scale fixed-bed column.

For large-scale processes, continuous systems are preferable and often more economical and effective [40], which motivates this work. Three steps govern the adsorption process in fixed beds: the external mass transfer, the internal diffusion and the adsorption itself, being the operational conditions, such as flow rate, bed depth and initial concentration of the contaminant of great relevance. The breakthrough curve, which describes the dynamic behavior and efficiency of a fixed-bed adsorption column [41], gives parameters that provide input information for modeling and future scale up of the system [7,42]. Generally, the breakthrough point is chosen as the point at which the concentration of adsorbate leaving the column reaches 5% of the initial concentration. However, this value can be chosen specifically for each application. Similarly, a concentration around 90–95% of the initial concentration can be used as a parameter to determine the exhaustion point [41]. The mass transfer zone (MTZ) is the region located between the breakthrough point and the point of exhaustion and it determines the region where mass transfer occurs within the column.

Therefore, this work aims at describing the use of bone char for the removal of refractory organics present in the electrodialysis saline concentrate effluent produced by petroleum refinery, using a lab-scale fixed-bed adsorption column. This represents a new contribution to support the association of reverse electrodialysis, evaporative crystallization, already in pilot-scale evaluation in an existent oil refinery, and adsorption, aiming at improving water recovery in oil refineries and an overall minimization of residues.

2. Experiments

2.1. Preparation of adsorbent and samples

2.1.1. Bone char

Bone char, supplied by Bonechar Carvão Ativado do Brasil, Maringá, Brazil, was produced at 700–750°C, in a furnace with limited supply of air for 8 h [17]. Sampling was carried out according to Brazilian technical standards [43] and particle size analysis was done by sieving in the vibrating system (Bertel Indústria Metalúrgica Ltda) using sieves of 6, 12, 32, 48, 60 and 100 mesh (6300, 3350, 1400, 500, 300 and 152 µm, respectively), for 15 min at 5 rpm. Particles of 12–32 mesh size (0.5–1.4 mm) were selected for the adsorption experiments, and prior to their use were washed four times using distilled water (2 L water/500 g of bone char) to remove any tiny particles adhered to their surfaces. Finally, bone char was dried in a furnace (Sterilifer SX1.1 DTME, series 0057) at 120°C for 2 h.

2.1.2. Electrodialysis concentrate effluent (C-EDR)

The real effluent used was obtained from the saline concentrate stream of electrodialysis, the last step of advanced wastewater treatment, in 10–20 L plastic flasks, after being appropriately cleaned, washed and rinsed. The characterization of the effluent was carried out according to Standard Methods for Analysis of Water and Wastewater [44]. Refractory organics qualitative characterization for equilibrium study was carried out at Federal University of São Paulo (USP) and determined by gas chromatography/mass spectrometry (GC/MS Shimadzu QP 2010 plus; capillary column

Agilent, DB-5MS 30m × 0.25 mm; injection volume 1 µL; heat flow rate 7°C/min, from 40°C to 310°C).

2.1.3. Dissolved organics determination

Dissolved organics were quantified using closed reflux, colorimetric method for low-concentration range of chemical oxygen demand (COD) as described in standard methods [44]. The absorbance was measured in a spectrophotometer (AJX 1600) at the wavelength of 420 nm. The organic concentration in the effluent, in terms of COD, was determined from an analytical curve for potassium biphthalate standards at concentrations of 10, 20, 30, 40, 50, 60 and 70 mg L^{-1}.

Previously to COD determination, samples were filtered through a 8-µm quantitative paper, and then, through 0.22-µm disposable membranes (Millipore Millex GV, hydrophilic PVDF 0.22 µm), so that bone char residuals and other suspended solids could be eliminated and only dissolved organics would be quantified.

2.2. Bench-scale fixed-bed adsorption experiments

Adsorption continuous tests were carried out in a polycarbonate fixed-bed column (12.9 cm height and internal diameter of 2.2 cm). Bone char was packaged between two layers of glass beads. In order to evaluate the effect of bed depth, five continuous experiments with fixed flow rate (Q) and initial concentration (C_0) (Q = 3.00 mL min^{-1} and C_0 = 63 mg L^{-1}) were carried out, but with varying bed depths (h = 2.6, 3.5, 5.0, 7.7 and 12.9 cm). In order to check the flow rate effect, bed height (h) and C_0 were kept constant (h = 7.7 cm and C_0 = 63 mg L^{-1}) and three flow rate conditions were compared (Q = 1.50, 3.00 and 6.00 mL min^{-1}). Finally, the effect of input organic concentration for C_0=63 and 93 mg L^{-1} was evaluated, keeping the flow rate and the bed depth constant at 6.00 mL min^{-1} and 7 cm, respectively. Temperature and pH were monitored (HANNA pH 21) in each run, being measured at least in triplicate. In order to guarantee homogeneity, C-EDR effluent was magnetically stirred (Thelga TMA10 CFI). The effluent was pumped upstream (MS Tecnopon Instrumentation DMC-100 peristaltic pump) through the bone char bed, as shown in Figure 1.

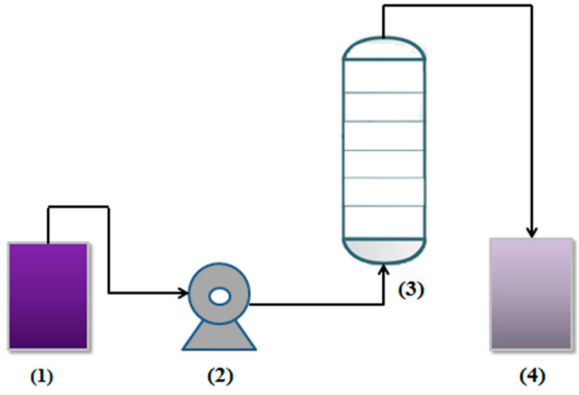

Figure 1. Experimental setup for the continuous tests in a lab-scale fixed-bed column: (1) effluent C-EDR under magnetic stirring; (2) peristaltic pump; (3) polycarbonate column and (4) treated effluent for filtration and analysis.

The operational parameters that describe the behavior of the breakthrough curves were calculated from the results. For determination of t_f and t_z, the volume of effluent at the breakthrough points was obtained considering C/C_0 5% higher than the initial C/C_0 ratio and the exhaustion times were determined taking 5% less than the final C/C_0 ratio.

The necessary time to move the adsorption zone through the adsorption column is given by [45]

$$t_z = \frac{V_E - V_b}{Q}, \tag{1}$$

where t_z is the necessary time to move the adsorption zone through the adsorption column (h), V_E is the effluent volume at the exhaustion point (L), V_b is the effluent volume at the breakpoint (L) and Q is the flow rate (L h^{-1}).

The time to establish the MTZ, or exhaustion time, t_E (h), was determined according to Equation (2) [45], where V_E is the volume of exhaustion (L) and Q is the volumetric flow rate (L h^{-1})

$$t_E = \frac{V_E}{Q}. \tag{2}$$

In order to calculate the time required for the adsorption zone to be initially formed, it was necessary to calculate the fractional capacity of the adsorbent in the adsorption zone, which is given by [45]

$$F = \frac{\int_{V_b}^{V_E} (C_0 - C)dV}{C_0(V_E - V_b)}, \tag{3}$$

where F is the fractional capacity of the adsorbent in the adsorption zone, C_0 is the effluent inlet concentration (mg L^{-1}) and C is the effluent concentration varying with the time.

The time required for the adsorption zone to be initially formed (t_f) may be obtained by [45]

$$t_f = (1 - F)t_z. \tag{4}$$

The moving adsorption zone rate (U) and the adsorption zone depth (cm) could be obtained by Equations (5) [45] and (6) [45], respectively, where U is the moving adsorption zone rate (cm/h), X is the total bed depth (cm) and X_z

is the adsorption zone depth (cm)

$$U = \frac{X_z}{t_z} = \frac{X}{t_E - t_f}, \quad (5)$$

$$X_z = \frac{X(t_z)}{t_E - t_f}. \quad (6)$$

Finally, the column saturation (S) is calculated as shown below [45]:

$$S(\%) = \frac{X + (F-1)X_z}{X} \times 100. \quad (7)$$

2.2.1. Determination of bed adsorptive capacities (q)

Bed adsorption capacities were calculated by numerical integration of experimental breakthrough curves, using Curve Expert® software, and taking into account the flow rate and bone char mass in the column for each experiment. The refractory amount of organics was subtracted from the total value obtained from the integration to determine the real value for q.

2.3. Mathematical modeling

Thomas (Equation (8)), Yan (Equation (9) and Equation (10)), Wolborska (Equations (11) and (12)), and bed depth service time (BDST) (Equations (13) and (14)) models were fitted to experimental data according to the literature [16,41,46–49]

$$\frac{C}{C_0} = \frac{1}{1 + \exp\left[\left(\frac{K_T q_e m}{Q}\right) - K_T C_0 t\right]}, \quad (8)$$

where K_T is the Thomas constant (L mg^{-1} min^{-1}), q_e is the maximum adsorption capacity (mg g^{-1}), C is the equilibrium concentration (mg L^{-1}) at time t (min), C_0 is the initial concentration (mg L^{-1}), m is the adsorbent mass (g), Q is the flow rate (mL min^{-1}) [41,49]

$$\frac{C}{C_0} = 1 - \frac{1}{1 + \left(\frac{Qt}{b}\right)^a}, \quad (9)$$

$$q_e = \frac{bC_0}{m}, \quad (10)$$

a, b are parameters of the Yan model, Q is the flow rate (mL min^{-1}), t is the time (min), m is the adsorbent mass (g), q_e is the bed capacity (mg g^{-1}); C is the equilibrium concentration (mg L^{-1}) at time t (min), C_0 is the initial concentration (mg L^{-1}) [46]

$$\frac{C}{C_0} = e^{(\beta_a C_0/N_0)t - \beta_a X/U}, \quad (11)$$

$$\beta_\alpha = \frac{U^2}{2D}\left(\sqrt{1 + \frac{4\beta_0 D}{U^2}} - 1\right), \quad (12)$$

where β_α is the external mass transfer kinetic coefficient (h^{-1}), D is the axial diffusion coefficient (cm^2 h^{-1}), β_0 is the external mass transfer kinetic coefficient for negligible axial diffusion coefficient, N_0 is the exchange capacity (mg L^{-1}), U is the superficial fluid velocity (cm h^{-1}) and X is the bed depth (cm) [47,48,50]

$$\ln\left(\frac{C_0}{C_b} - 1\right) = \ln(e^{(K_a \cdot N_0 \cdot X)/U} - 1) - K_a \cdot C_0 \cdot t, \quad (13)$$

$$t = \frac{N_0}{C_0 U}X - \frac{1}{C_0 K_a}\ln\left(\frac{C_0}{C_b} - 1\right), \quad (14)$$

where C_0 is the initial solute concentration (mg L^{-1}), C_b is the concentration at breakthrough point (mg L^{-1}), K_a is the adsorption rate constant (L mg^{-1} h^{-1}), N_0 is the adsorption capacity (mg L^{-1}), X is the bed depth (cm), U is the linear flow velocity (cm h^{-1}), t is the column service time (h) [16].

After the determination of the BDST equation for a specific flow rate and initial concentration, the BDST model was fitted for different C/C_0 ratios (0.25, 0.30, 0.55, 0.60 and 0.65), for bed depths of 5.0, 7.7 and 12.9 cm and flow rate of 2.97 ± 0.03 mL min^{-1}. The equations for each C/C_0 condition were acquired by a linear fit. The angular (a) and linear (b) coefficients, K_{BDST} and N_0 values were determined by the following equations:

$$a = \frac{N_0}{C_0 U}, \quad (15)$$

$$b = \frac{1}{C_0 K_a}\ln\left(\frac{C_0}{C_b} - 1\right). \quad (16)$$

Equation (17) was used to determine the critical bed depth, X_0, the minimum required for the final adsorbate concentration at the outlet of the column to be C_b:

$$X_0 = \frac{U}{N_0 K_a}\ln\left(\frac{C_0}{C_b} - 1\right). \quad (17)$$

In order to evaluate the fit obtained by the BDST model, values of the times required to reach the same C/C_0 ratios, for a bed depth of 7.7 cm, but at a different flow rate (1.5 ± 0.04 mL min^{-1}) were calculated and compared to experimental data. The deviation was estimated according to the following equation:

$$\text{Deviation}\% = \frac{(T_{exp} - T_{model})}{T_{exp}}, \quad (18)$$

where deviation (%) is the percentage difference

between the predicted time (T_{model}) and that obtained experimentally (T_{exp}).

From the BDST model, the system was scaled up assuming the operational conditions for one industrial column, of area 6.15 m^2, internal diameter of 2.80 m, column height of 1.50 m, completely full of bone char, to treat refractory organics from C-EDR effluent at a flow rate of 13 $m^3\ h^{-1}$ and the initial COD concentration of 61.11 mg L^{-1}. These industrial operational conditions were considered for scaling up based on the dimensions of inactive carbon filters already existent in the refinery, as well as on the operational conditions for the concentrate stream produced by electrodialysis in the real process.

3. Results and discussion

3.1. Breakthrough curves and bed capacities

The breakthrough curves were obtained for different operational conditions in continuous experiments using bone char in a fixed-bed column for C-EDR refractory organics removal, as shown in Table 1 and in Figures 2–4.

It is interesting to note different patterns in the shape of breakthrough curve for the system. This can be especially highlighted in Figure 2(e), condition under which the column worked completely full of bone char (bed depth = column height), the curve ongoing at C/C_0 at approximately 0.2, differently from what is normally expected and reported in the literature, C/C_0 starting from zero (0). An ideal rupture curve assumes a total adsorption of the adsorbate between the initial stages of operation and the point of rupture (C_b). According to Metcalf & Eddy [7], when the breakthrough curve does not start from 0 (zero), the presence of compounds that can be adsorbed and others which cannot be adsorbed is indicated [7]. In other words, the C-EDR contained organics that bone char was not able to retain. In fact, this was confirmed by GC/MS analysis for previous equilibrium studies, when it was observed that after the equilibrium was reached, some of the 70 organic compounds present in C-EDR were also present in the treated C-EDR, the maximum removal being achieved at around 60% ($C/C_0 = 0.4$) for equilibrium conditions. The influent was a mixture of long-chain hydrocarbons, mostly alkanes and alkenes. Indeed, alkanes are not very reactive and have low biological activity, the reason why they were found in the concentrate stream. In addition, aromatics, carboxylic acids, amines and amides had also been identified [51]. The most pronounced peaks were: 9-octadecenamide, (*Z*)-docosane, 1,22-dibromo-, hexadecane, d-ribose, 2-deoxy-bis(thioheptyl)-, eicosanoic acid, 2,3-bis[(trimethylsilyl)oxy]propyl ester, octadecanoic acid, 3-oxo-, methyl ester, phenol, 2,4-bis(1,1-dimethylethyl)-, undecane, 4-ethyl-, 1*H*-indene, 1-hexadecyl-2,3-dihydro. After adsorption, it was observed that, from the 70 refractory organics in the influent, 25 were not identified in the effluent any longer; therefore, they had been retained onto the bone char.

Another curious point to consider is about the shape of the breakthrough curve, shown in Figure 2(e), which did not follow the exact sigmoidal form reported by the literature. In fact, COD removal curves throughout the entire experiment for the completely filled column (11 days) seemed to be an assembly of several sigmoidal breakthrough curves. C/C_0 started at approximately 0.15–0.20 and stabilized for the first time around $C/C_0 = 0.45$. After this time, the organic concentration in the treated effluent remained approximately constant, suggesting a possible exhaustion. However, after 115 h (almost 5 days) of experiment, C/C_0 began to increase again, until new steadying was reached, around $C/C_0 =$ 0.65, 0.70. After about 190 h (or ~8 days) of experiment, C/C_0 arose again, reaching its last level of stability at about $C/C_0 = 0.85$. This behavior reinforced the hypothesis of adsorption in multilayers, in which each layer of adsorbate constitutes new adsorption sites. Literature

Table 1. Operational conditions of the continuous tests to verify the interference of bed depth (*X*), flow rate (*Q*) and initial concentration of organics, in terms of COD (C_0) on the adsorptive process: desired values and measured values.

X (cm)	Flow rate, *Q* (goal) (mL min^{-1})	Flow rate, *Q* (real) (mL min^{-1})	C_0 (goal) (mg L^{-1})	C_0 (real) (mg L^{-1})	pH	*T* (°C)	Figure
Bed depth influence							
2.6	3.00	3.09 ± 0.04	63	67 ± 9	7.8 ± 0.2	22.7 ± 0.8	2(a)
3.5	3.00	3.07 ± 0.07	63	65 ± 3	7.7 ± 0.1	24 ± 1	2(b)
5.0	3.00	3.00 ± 0.15	63	60 ± 5	7.7 ± 0.2	22 ± 1	2(c)
7.7	3.00	2.94 ± 0.05	63	66 ± 1	7.7 ± 0.2	23.9 ± 0.7	2(d)
12.9*	3.00	2.98 ± 0.09	63	60 ± 1	7.9 ± 0.4	26 ± 2	2(e)
Flow rate influence							
7.7	1.50	1.50 ± 0.04	63	62 ± 5	8.3 ± 0.3	25 ± 2	3(a)
7.7	3.00	2.94 ± 0.05	63	66 ± 1	7.7 ± 0.2	23.9 ± 0.7	3(b)
7.7	6.00	5.81 ± 0.16	63	62 ± 8	7.4 ± 0.4	25 ± 2	3(c)
Initial concentration influence							
7.7	6.00	5.81 ± 0.16	63	62 ± 8	7.4 ± 0.4	25 ± 2	4(a)
7.7	6.00	6.15 ± 0.19	93	93 ± 1	8.2 ± 0.3	25 ± 2	4(b)

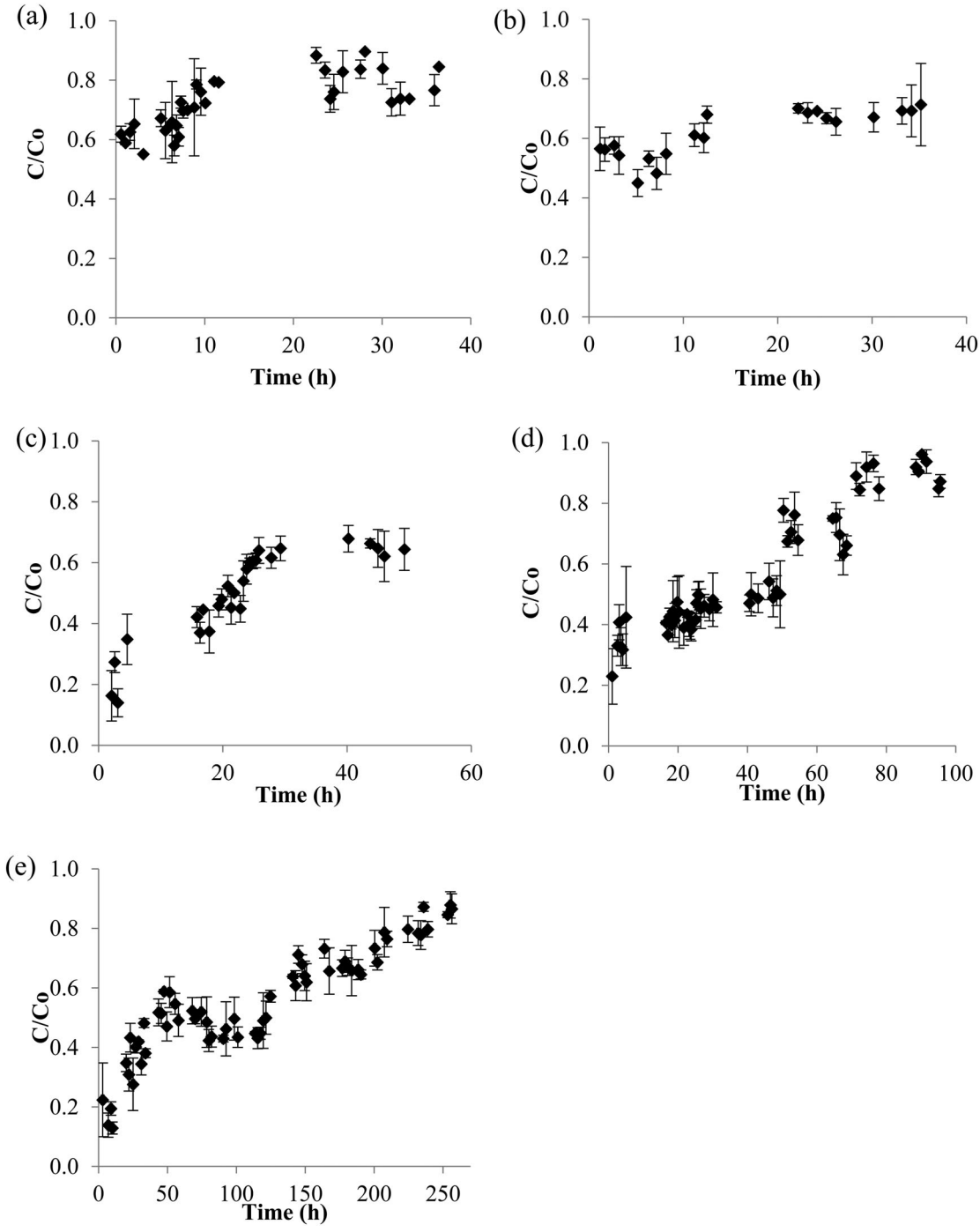

Figure 2. Breakthrough curves for different bed depths obtained in lab-scale fixed-bed experiments. $C_0 = 63 \pm 4$ mg L^{-1}; $Q = 3.01 \pm 0.06$ mL min^{-1}: (a) $Z = 2.6$ cm; (b) $Z = 3.5$ cm; (c) $Z = 5.0$ cm; (d) $Z = 7.7$ cm; (e) $Z = 12.9$ cm.

reports that since the main phase present in bone char is hydroxyapatite, most surface groups (phosphates, hydroxyls and carbonates) are negative at pH above 5 [22,39], which was the case in this investigation. Therefore, at the beginning, possible interactions with the organic compounds would occur through hydrogen bonds between electronegative heteroatoms such as oxygen, present in the phosphate, carbonate and hydroxyl groups of bone char, and hydrogen from O–H and N–H of the carboxylic acids, phenols, amines and amides contained in the effluent. Then, weak interactions, such as van der Waals, among long chains of hydrocarbons adhered to the solid, could be present [51]. In fact, the type of isotherm obtained from bone char characterization for determination of surface area and porosity by the Brunauer–Emmet–Teller method was the type 5 isotherm [51], typical for relatively weak adsorbate–adsorbent interactions [51,52]. Therefore,

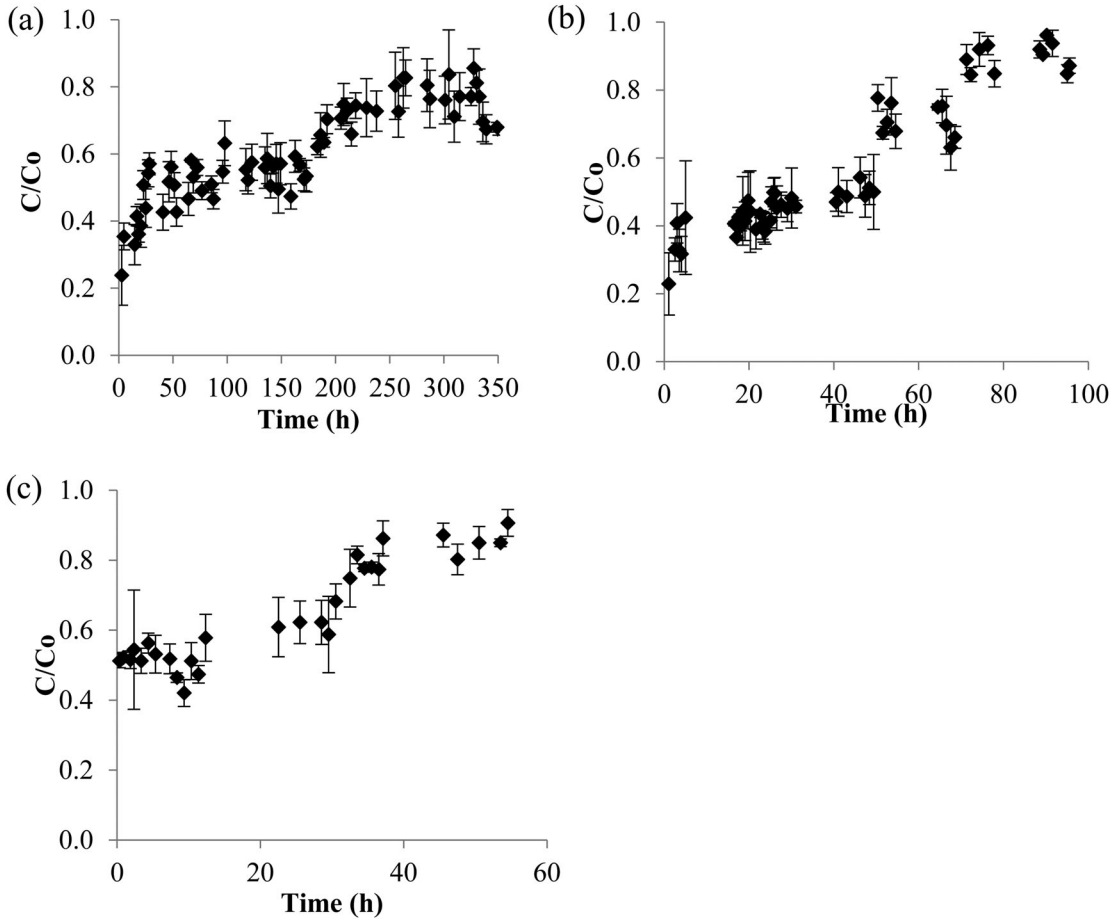

Figure 3. Breakthrough curves for different flow rates obtained in lab-scale fixed-bed experiments. $C_0 = 63 \pm 4$ mg L^{-1}; $Z = 7.7$ cm: (a) $Q = 1.50 \pm 0.04$ mL min^{-1}; (b) $Q = 2.94 \pm 0.05$ mL min^{-1} and (c) $Q = 5.81 \pm 0.16$ mL min^{-1}.

there was formation of a first layer, on the surface of the adsorbent, until its complete saturation occurred ('first' breakthrough). From this moment, the adsorption zone was occupied until its 'first' exhaustion occurred. When the bed was exhausted, the concentration of the treated effluent was not affected any longer. Nevertheless, as more and more effluent flew upstream through the column and more organics contacted the bone char, new active sites appeared by the overlapping of long-chain C-EDR compounds. It seemed that the process restarted, adsorption continued leading to a new saturation (and, therefore, a new breakthrough

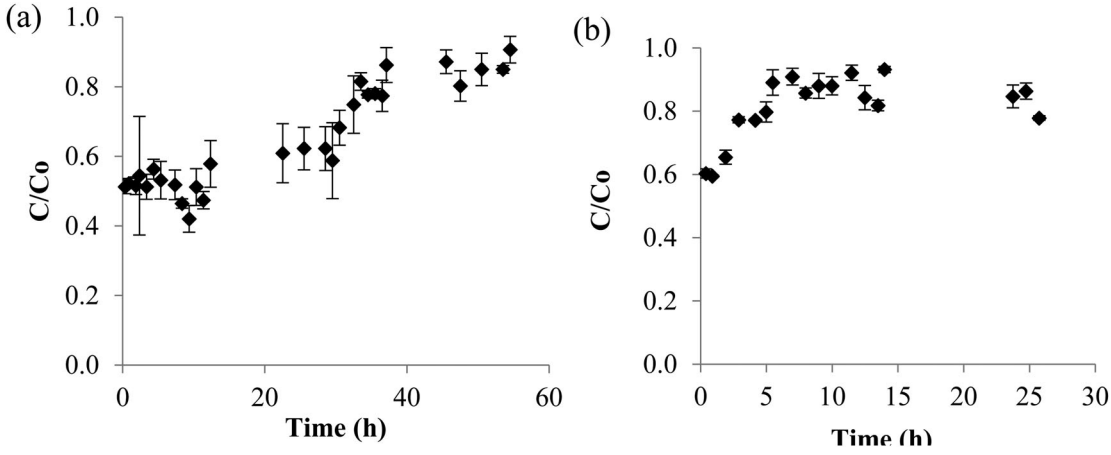

Figure 4. Breakthrough curves for different initial C-EDR COD concentrations obtained in lab-scale fixed-bed experiments. $Q = 5.98$ mL min^{-1}; $Z = 7.7$ cm: (a) $C_0 = 62 \pm 8$ mg L^{-1} and (b) $C_0 = 93 \pm 1$ mg L^{-1}.

point) and new exhaustion. This was repeated three times for the deepest bed possible at the experimental conditions. At lower bed depths, the breakthrough curves obtained seemed to be portions of the complete curve, for a bed depth of 12.9 cm. For 7.7 cm depth, it was possible to notice two distinct regions and the entire range of C/C_0 (from 0.2 to 0.9) was also observed, in stages of breakthrough and exhaustion, but with shorter times and smaller volumes of treated effluent. When the bed depth was 5.0 cm, the curve started at 0.20 and stabilized at approximately 0.65, only two regions could be observed. At lower bed depths (Z = 3.5 and 2.6 cm), it was not possible to observe either the breakthrough or C/C_0 regions before 0.5, 0.6, going to 0.7 and 0.85, respectively. Therefore, as mentioned by McCabe et al. [53], deep bed layers affected the treatment efficiency, since the adsorption rate in liquids is slower when compared to the gas adsorption.

Concerning bed capacities, a variation from around 6.00 to 35.60 mg g^{-1} was observed for the different bed depths applied, as shown in Table 2. The maximum value of q (35.60 mg g^{-1}) obtained for the deepest bed (12.9 cm) was due to the larger amount of the adsorbent, which resulted in a greater availability of active sites to adsorb organics [54] and superior opportunity of adsorbent–adsorbate.

A breakthrough curve profile very similar to that obtained for bed depth variation could be observed due to flow rate variations. At low flow rates, for example, the curves seemed to be composed of more than one breakthrough–exhaustion region, suggesting once again the recovery of adsorptive capacity over time (or with greater volume of treated effluent), with more adsorbate being incorporated (multilayers). The lowest flow rate (1.5 mL min^{-1}) was the condition under which higher levels of removal were achieved (q = 29.95 mg g^{-1}), since the curve started from C/C_0 of approximately 0.20, reaching 0.85 in the 'last' exhaustion. Indeed, as can be seen in Table 3, bed adsorption capacity almost doubled when the lowest flow rate (Q = 1.5 mL min^{-1}) was compared to Q = 2.94 mL min^{-1} (29.95 against 15.39 mg g^{-1}, respectively) and was more than three times superior, when compared to Q = 5.81 mL min^{-1}. This increase was due to greater residence time of the solution inside the column when smaller flow rates were employed [46], which also favored the adsorbent–adsorbate contact.

Evaluating the influence of the initial concentration of organics, bed capacities did not vary significantly for the range of Co investigated, as they differed less than 5% in the conditions tested (X = 7.7 cm and Q ~6.0 mL min^{-1}), from 8.80 to 9.29 mg g^{-1} from Co ~ 63 mg L^{-1} to Co = 93 mg L^{-1}, respectively.

The operational parameters describing the breakthrough curve obtained from each experimental condition, calculated from the equations presented in the previous section, are shown in Table 4. The breakthrough points were determined considering C/C_0 5% higher than the initial C/C_0 ratio, in each region of the curve. The exhaustion times were determined taking 95% of the final C/C_0 ratio for each region.

For those conditions where more than one breakthrough–exhaustion region was noticed, the curve was sectioned in each region and the parameters obtained were calculated for each of the regions. The time to the MTZ to move, tz, was proportional to the volume of treated effluent between the breakthrough point and the point of exhaustion, and this value increased with the rise of bed depth, with the reduction of the flow rate and initial concentration.

Regarding the bed depth, breakthrough curves became steeper when the bed depth diminished, indicating a reduction in mass transfer resistance [41]. In addition, breakthrough time increased with growing bed depth. This was due to the larger amount of the adsorbent, which resulted in a greater availability of active sites to adsorb organics [54] and due to solution residence time increasing inside the column [46], favoring adsorbent–adsorbate contact, as discussed previously. Regarding the flow rate, breakthrough was reached more quickly when the flow rate increased. This was because, as the flow rate increases, mass transfer resistance decreases. Therefore, it was notorious that the service time increased with the reduction of flow rate, leading to a greater volume of effluent treated up to the breakthrough point. Liu et al. stated that flow rate is an important issue to control the delay factor, residence time and hydraulic conductivity in a treatment system and its increase raises the rates of external mass transfer and internal diffusion, leading to a faster saturation compared to lower flow rates [55], what was observed in this study.

Column saturation up to breakthrough point increased with the decrease of adsorption zone depth,

Table 2. Bed adsorptive capacities for different bed depths (Q ~ 3.0 mL min^{-1} and C_0 ~ 63.0 mg L^{-1}).

Operational conditions (goals)	Q ~ 3.0 mL min^{-1} and C_0 ~ 63.0 mg L^{-1}				
Bed depths, X (cm)	2.6	3.5	5.0	7.7	12.9
Adsorptive capacity, q (mg g^{-1})	7.24	5.96	12.00	15.39	35.60

Table 3. Bed adsorptive capacities for different flow rates (X = 7.7cm and C_0 ~ 63.0 mg L^{-1}).

Operational conditions (goals)	X = 7.7 cm and C_0 ~ 63.0 mg L^{-1}		
Q (mL min^{-1})	1.50	2.94	5.81
q (mg g^{-1})	29.95	15.39	8.80

Table 4. Operational parameters to describe breakthrough for bone char-C-EDR refractory organics system.

Bed depth	X (cm) (regions)	2.6	3.5	5.0[a] (1)	5.0[a] (2)	7.7[a] (1)	7.7[a] (2)	7.7[a] (1)	7.7[a] (2)	7.7	7.7	12.9[a] (1)	12.9[a] (2)	12.9[a] (3)
Flow rate	Q (mL min^{-1})	3.09 ± 0.04	3.07 ± 0.07	3.00 ± 0.15	3.00 ± 0.15	1.50 ± 0.04	1.50 ± 0.04	2.94 ± 0.05	2.94 ± 0.05	5.81 ± 0.16	6.15 ± 0.19	2.98 ± 0.09	2.98 ± 0.09	2.98 ± 0.09
Initial concentration	C_0 (mg L^{-1})	67 ± 9	65 ± 3	60 ± 5	60 ± 5	62 ± 5	62 ± 5	66 ± 1	66 ± 1	62 ± 8	93 ± 1	60 ± 1	60 ± 1	60 ± 1
Breakthrough time	t_b (h)	2.5	9.0	2.0	15.5	10	170	1	26	12	3	8	120	200
Exhaustion time	t_e (h)	9.0	12.0	4.0	25.0	20	200	3	72	33	5	30	150	250
Time to move MTZ	t_z (h)	6.5	3.0	2.0	9.5	10	30	2	46	21	2	22	30	50
Bed depth/time	U_z(cm/h)	0.54	0.34	1.49	0.25	0.45	0.04	3.17	0.17	0.39	2.25	0.56	0.10	0.06
Adsorption zone depth	X_z (cm)	3.52	1.03	2.99	2.36	4.45	1.28	6.33	7.93	8.25	4.50	12.39	2.94	3.10
Column saturation	%S	12.5	82.7	80.6	75.7	84.3	89.5	76.6	38.9	31.6	53.9	69.0	85.9	80.0

[a]Conditions for which breakthrough curves were splitted in two or three regions of breakthrough/exhaustion, results per region.

with the increase of the flow rate and increase of the initial concentration. Gupta et al. also found the same trend while studying the removal of heavy metal ions in columns using an activated carbon from fertilizer residues [45] as adsorbent.

3.2. Mathematical modeling

Thomas, Yan, Wolborska and BDST models were fitted to experimental data and this mathematical modeling showed precarious fitting ($R^2 < 0.90$) for most cases. The Yan model fit was poor for all the operational conditions ($R^2 < 0.90$), thus, Yan parameters results were suppressed. Thomas, Wolborska and BDST models also failed to describe the system for the conditions of lower bed depths (2.6, 3.5 and 5.0 cm), highest initial concentration ($C_0 = 93 \pm 1$) and lowest flow rate ($Q = 1.50 \pm 0.04$). Nevertheless, for the operational conditions under which the determination coefficient R^2 was around 0.90 or superior for Thomas, Wolborska and BDST modeling, the parameters obtained are presented in Table 5. Such operational conditions also allowed comparison of bed depths and flow rates effect.

As far as Thomas, Wolborska and BDST models are concerned, it can be highlighted that, as mentioned by Xu et al., every model has its limitations because they are derived from specific conditions and situations. Moreover, still according to Xu et al. [16], 'breakthrough curves deviate from the ideal S shape, prediction derived from any model usually cannot meet the demands' (p. 172) and, as discussed previously, this was the case in this study.

The Thomas model, for example, in spite of being one of the most widely used models, as mentioned by Lezehari et al. and Song et al. [48,56,57], was developed to describe mathematically the performance of a cation exchange column. It presents a relatively general flowing system equation, assuming the second-order reversible reaction kinetics (which was the case in the real system, one of the reasons why the Thomas model was tested). The model neglects axial dispersion effects and in this study, we could admit that axial dispersion was not relevant for Thomas model fitting. In this study, despite L (bed length)/D (internal diameter) ratio was close to 6, far from the ratio $L/D > 20$, value cited in the literature as the conservative value to guarantee that axial dispersion can be neglected, some authors take negligible axial dispersion into account at lower L/D values, depending on other characteristics of the system and operational conditions. *Apud* Delgado [58] mentions that the variations of the fluid velocity, porosity and dispersion coefficient, in radial position, can be negligible if D (column diameter)/d (particle diameter) > 15, which was the case in this

Table 5. Thomas, Wolborska and BDST parameters for different operational conditions (values whose $R^2 > 0.90$).

Bed depth, X (cm)	Flow rate, Q (mL min^{-1})	Initial COD C_0 (mg L^{-1})	Thomas parameters (non-linear model)			Wolborska parameters (non-linear model)			BDST parameters (non-linear model)		
			K (L (mg h)$^{-1}$)	Q_0 (mg g^{-1})	R^2	β (h^{-1})	N_0 (mg L^{-1})	R^2	K (L mg^{-1} h^{-1})	N_0 (mg L^{-1})	R^2
7.7	2.94 ± 0.05	66 ± 1	0.00048	13.01	0.9381	6.50	38,050	0.9404	0.00048	12,444	0.9381
12.9	2.98 ± 0.09	60 ± 1	0.00015	22.92	0.9022	3.86	62,962	0.8985	0.00015	19,761	0.9022
7.7	5.81 ± 0.16	62 ± 8	0.00058	4.41	0.9175	8.67	45,676	0.9279	0.00058	3474	0.9175

study (D/d~23). Celenza reports as usual a ratio $L/D > 4$ [58,59].

Modeling according to Wolborska was tried because of the real system investigated in this study and Wolborska and Wolborska and Pustelnik studied the adsorption of an organic compound (*p*-nitrophenol) on activated carbon [16,60,61].

The BDST model is derived from the Bohart–Adams model and they have been successful in predicting several breakthrough curves [16,48,62]. Due to its simplicity associated with the assumption that adsorption is governed by the surface reaction between the adsorbate and the unused capacity of the adsorbent, this model was used in the present work, also aiming at providing helpful information to scale up the process as it is discussed in the following section.

From Table 5 analysis, it was observed that, although numerical values of adsorption capacity parameters obtained by the Thomas model were diverse from real ones due to the fit, the same trend as observed for calculated capacity values was confirmed: deeper beds and low flow rates give better results of adsorption capacity. This trend was similar to that found by Singh et al. in their continuous adsorption studies, for the removal of furfural, from aqueous solutions using activated charcoal as adsorbent [63]. Indeed, as the bed depth increased and the flow rate decreased, the residence time of the solution in the column became larger, allowing the diffusion of the adsorbate deeper into the porous of the adsorbent, so that both the saturation time and the capacity of adsorption increased [46]. From the results with higher determination coefficients for BDST modeling, it was noticed that the increase in bed depth and the decrease in the flow rate led to a reduction in the adsorption rate, indicating that the process became slower. In fact, the reduction of the rate contributed to the increase of adsorption capacity by improving the adsorbent–adsorbate contact. For Wolborska parameters, the same conclusions could be drawn for the effects of bed depth and flow rate, in cases where the fit was satisfactory. β parameter decreased for greater bed and lower flow rate; then, mass transfer occurred more slowly in these cases, corroborating previous discussions. In fact, Hamdaoui stated that the increase in the flow rate increases β, since there is a decrease of the boundary layer around the adsorbent with higher turbulence [47].

The effect of the initial concentration on the maximum adsorptive capacity obtained by the models could not be evaluated, since the fit to all the models for these conditions was precarious ($R^2 = 0.4494$).

3.3. Scale up

Figure 5 shows the BDST model for different C/C_0 ratios (0.25, 0.30, 0.55, 0.60 and 0.65) for bed depths of 5.0, 7.7 and 12.9 cm at a flow rate of 2.97 ± 0.03 mL min^{-1}. From the angular and linear coefficients obtained for each C/C_0 ratio, K_{BDST} and N_0 were calculated as described in the experimental section. Critical depth (X_0) was determined and the results are shown in Table 6.

The best fit was observed for C/C_0 of 0.55. Calculated critical depths (X_0) confirmed experimental results, for example, for $C/C_0 = 0.25$, X_0 was 4.87 cm and at bed heights of 2.6 and 3.5 cm it was only possible to identify the breakthrough curve from $C/C_0 = 0.60$ and 0.55, respectively; and at 5.0 cm bed depth, $C/C_0 = 0.25$ was identified. For $C/C_0 = 0.55$ (best fit), the predicted critical depth was 3.6 cm. In fact, at 3.5 cm bed depth, experimentally evaluated, it was possible to identify C/C_0 of 0.55 (which was not the case at lower depth, such as that of 2.6 cm). For the BDST scale-up method, validation testing at a lower flow rate ($Q = 1.5 \pm 0.04$ mL min^{-1}) was carried out and deviation between theoretical and experimental values is presented in Table 7.

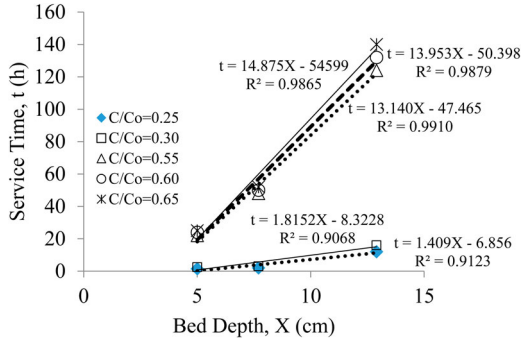

Figure 5. Bed depth service time model for bed depths of 5.0, 7.7 and 12.9 cm and flow rate of 2.97 ± 0.03 mL min^{-1} with C/C_0 of 0.25, 0.30, 0.55, 0.60 and 0.65.

Table 6. BDST model parameters for different C/C_0.

C/C_0	K_{BDST} (L mg^{-1} h^{-1})	N_0 (mg L^{-1})	X_0 (cm)	R^2
0.25	2.62×10^{-3}	4038.18	4.87	0.9123
0.30	1.67×10^{-3}	5202.71	4.59	0.9068
0.55	-6.92×10^{-5}	37,661.74	3.61	0.9910
0.60	-13.2×10^{-5}	39,991.95	3.61	0.9879
0.65	-18.6×10^{-5}	42,634.58	3.67	0.9865

Table 7. Column service time for $C/C_0 = 0.25$, 0.30, 0.55, 0.60 and 0.65: model (previewed by BDST model) and experimental (through breakthrough curves, $h = 7.7$ cm and $Q = 1.5 \pm 0.04$ mL min^{-1}).

Time (h) to reach C/C_0	Experimental	Model	Deviation (%)
0.25[a]	7.00	14.62	−108.86*
0.30[a]	14.00	19.35	−38.21*
0.55	172.00	152.87	11.12
0.60	180.00	162.33	9.82
0.65	188.00	172.18	8.41

[a]Huge deviations, more than 30%.

For C/C_0 of 0.25 and 0.30, the deviations were huge (more than 100% for the first case and more than 35% for the second case). On the other hand, a deviation close to 10% was observed for prediction of breakthrough time by theoretical calculation for C/C_0 of 0.55, 0.60 and 0.65, which can be considered acceptable, since C-EDR effluent is a real complex mixture of organic and inorganic compounds on which several intervening factors can act [11]. Thus, the last three C/C_0 ratios were taken for scaling up and results are presented in Table 8. Therefore, scaling up predicted a service time for a single adsorption column operating under the above-mentioned conditions of about 16 days to reach 45% efficiency of removal of refractory organic ($C/C_0 = 0.55$) in terms of COD.

4. Conclusions

Refractory organics from saline stream from electrodialysis (C-EDR) were partially removed by bone char in an adsorption column in a lab scale. The effluent C-EDR contained organic compounds with opposite affinity by the bone char in the conditions employed. The maximum adsorption capacity of organics by bone char (q) increased with increasing bed depth and decreasing flow rate, due to the greater availability of active sites and greater adsorbent–adsorbate contact, reaching 35.60 mg g^{-1} for the deepest bed evaluated (12.9 cm) (at $Q \sim 3.0$ mL min^{-1} and Co $\sim$ 63.0 mg L^{-1}). Variation in the initial concentration did not affect the bed capacity significantly in the range of Co employed. It was possible to predict satisfactorily the breakthrough time by the BDST model (deviation near 10%) for C/C_0 of 0.55, 0.60 and 0.65, which was considered a very good result, due to the complexity of the effluent. Scaling up for a single adsorption column using real process conditions and dimensions of an inactive carbon filter already existent in the refinery predicted a service time of 16 days to remove, with 45% of efficiency ($C/C_0 = 0.55$), the refractory organics present in the effluent.

Table 8. Scale up for adsorption column to remove refractory organics from C-EDR effluent using bone char.

C/C_0	Time (h)	Time (days)
0.25[a]	40.07	1.67
0.30[a]	52.13	2.17
0.55	390.18	16.26
0.60	414.32	17.26
0.65	440.83	18.37

[a]High deviation predictions.

Note: Service time for different C/C_0 taking into account one-stage adsorption column of area $A = 6.15$ m^2; inner diameter Ø = 2.80 m. Bone char bed depth $h = 1.50$ m; to treat C-EDR.

Acknowledgements

The authors gratefully acknowledge University of São Paulo (USP), Bonechar Carvão Ativado do Brasil and Petrobras.

Disclosure statement

No potential conflict of interest was reported by the authors.

Funding

The authors gratefully acknowledge Brazilian Agencies CNPq (Conselho Nacional de Desenvolvimento Científico e Tecnológico) [482165/2013-8], FAPEMIG (Fundação de Amparo à Pesquisa do Estado de Minas Gerais) [APQ0268814], and CAPES-PROEX (Comissão de Aperfeiçoamento de Pessoal do Nível Superior - Programa de Excelência Acadêmica) for financial support.

References

[1] WWAP – United Nations World Water Assessment Programme. The United Nations world water development report 2016: water and jobs. Paris: UNESCO; 2016.
[2] Mekonnen MM, Hoekstra AY. Four billion people facing severe water scarcity. Sci Adv. 2016;2(2):e1500323–e1500323.
[3] Paranychianakis NV, Salgot M, Snyder SA, et al. Water reuse in EU states: necessity for uniform criteria to mitigate human and environmental risks. Crit Rev Environ Sci Technol. 2015;45:1409–1468.
[4] Alva-Argáez A, Kokossis AC, Smith R. The design of water-using systems in petroleum refining using a water-pinch decomposition. Chem Eng J. 2007;128:33–46.
[5] Souza BM, Souza BS, Guimarães TM, et al. Removal of recalcitrant organic matter content in wastewater by means of AOPs aiming industrial water reuse. Environ Sci Pollut Res. 2016;23:22947–22956.

[6] Garcia N, Moreno J, Cartmell E, et al. The application of microfiltration-reverse osmosis/nanofiltration to trace organics removal for municipal wastewater reuse. Environ Technol. 2013;34:3183–3189.
[7] Metcalf & Eddy, Revised by Tchobanoglous G, Stensel HD, Burton F. Wastewater engineering: treatment and resource recovery. 5th ed. New York, NY: McGraw-Hill Education; 2014.
[8] Diya-uddeen BH, Wan Daud WMA, Abdul Aziz AR. Treatment technologies for petroleum refinery effluents: a review. Process Saf Environ Prot. 2011;89(2):95–105.
[9] Santiago VMJ. Pesquisas e implantação de tecnologias de ponta no tratamento e reúso de efluentes hídricos em refinarias. VII Simpósio Internacional de Qualidade Ambiental. [Researches and implementation of new technologies for wastewater treatment and reuse in oil refineries. VII International Symposium on Environmental Quality]. Porto Alegre, RS; 2010.
[10] Ravanchi MT, Kaghazchi T, Kargari A. Application of membrane separation processes in petrochemical industry: a review. Desalination. 2009;235:199–244.
[11] Becheleni EMA, Borba RP, Seckler MM, et al. Water recovery from saline streams produced by electrodialysis. Environ Technol. 2015;36(3):386–394.
[12] Botalova O, Schwarzbauer J, Frauenrath T, et al. Identification and chemical characterization of specific organic constituents of petrochemical effluents. Water Res. 2009;43(15):3797–3812.
[13] Bhatnagar A, Kumar E, Sillanpaa M. Fluoride removal from water by adsorption: a review. Chem Eng J. 2011;171:811–840.
[14] Hashemi S, Rezaee A, Nikodel M, et al. Equilibrium and kinetic studies on the adsorption of sodium dodecyl sulfate from aqueous solution using bone char. Reac Kinet Mech Cat. 2013;109:433–446.
[15] Brunson LR, Sabatini DA. Practical considerations, column studies and natural organic material competition for fluoride removal with bone char and aluminium amended materials in the Main Ethiopian Rift Valley. Sci Total Environ. 2014;488–489:580–587.
[16] Xu Z, Cai J, Pan B. Mathematically modeling fixed-bed adsorption in aqueous systems. J Zhejiang Univ Sci A. 2013;14: 155–176.
[17] Nigri EM. Caracterização e estudo do mecanismo de sorção de fluoretos em carvão de osso. [Characterization and study of sorption mechanism of fluoride uptake by bone char]. Escola de Engenharia, Universidade Federal de Minas Gerais. Tese de doutorado em Engenharia Metalúrgica, de Materiais e de Minas [PhD Diss. on Metallurgical, Materials and Mining Engineering. Engineering School, Federal University of Minas Gerais, Brazil]. Belo Horizonte, MG; 2016.
[18] El-Refaey AA, Mahmoud AH, Saleh ME. Bone biochar as a renewable and efficient P fertilizer: a comparative study. Alex J Agric Res. 2015;60(3):127–137.
[19] Iriarte-Velasco U, Ayastuy JL, Zudaire L, et al. An insight into the reactions occurring during the chemical activation of bone char. Chem Eng J. 2014;251:217–227.
[20] Rojas-Mayorga CK, Bonilla-Petriciolet A, Aguayo-Villarreal IA, et al. Optimization of pyrolysis conditions and adsorption properties of bone char for fluoride removal from water. J Anal Appl Pyrol. 2013;104:10–18.
[21] Tovar-Gómez R, Moreno-Virgen MR, Dena-AGuilar JA, et al. Modeling of fixed-bed adsorption of fluoride on bone char using a hybrid neural network approach. Chem Eng J. 2013;228:1098–1109.
[22] Rocha SDF, Ribeiro MV, Viana PRM, et al. Bone char: an alternative for removal of diverse organic and inorganic compounds from industrial wastewater. In: Amit Bhatnagar (Org.). Application of Adsorbents for Water Pollution: Bentham Science; 2011, v. 14. Available from: http://www.benthamscience.com/ebooks/forthcomingtitles.htm
[23] Ghanizadeh GH, Asgari G. Adsorption kinetics and isotherm of methylene blue and its removal from aqueous solution using bone charcoal. Reac Kinet Mech Cat. 2011;102:127–142.
[24] Moreno-Piraján JC, Gómez R, Giraldo L. Removal of Mn, Fe, Ni and Cu ions from wastewater using cow bone charcoal. Materials. 2010;3:452–466.
[25] Rezaee A, Ghanizadeh GH, Behzadiyannejad GH, et al. Adsorption of endotoxin from aqueous solution using bone char. Bull Environ Contam Toxicol. 2009;82:732–737.
[26] Yun-Nen C, Li-yuan C, Yu-De S. Study of arsenic (V) adsorption on bone char from aqueous solution. J Hazard Mater. 2008;160:168–172.
[27] Choy KKH, McKay G. Sorption of cadmium, cooper, and zinc ions onto bone char using Crank diffusion model. Chemosphere. 2005;60(8):1141–1150.
[28] Cheung CW, Choy KKH, Ko DCK, et al. Sorption equilibria of metal ions on bone char. Chemosphere. 2004;54 (3):273–281.
[29] Wilson JA, Pulford ID, Thomas S. Sorption of Cu and Zn by bone charcoal. Environ Geochem Health. 2003;25:51–56.
[30] Dahbi S, Azzi M, de La Guardia M. Removal of hexavalent chromium from wastewaters by bone charcoal. Fresenius' J Anal Chem. 1999;363:404–407.
[31] Rezaee A, Ramin M, Nili-Ahmadabadi A. Adsorption of Escherichia coli using bone char. J Appl Sci Environ Manage. 2011;15(1):57–62.
[32] Ip AWM, Barford JP, McKay G. Biodegradation of reactive black 5 and bioregeneration in upflow fixed bed bioreactors packed with different adsorbents. J Chem Technol Biotechnol. 2010;85:658–667.
[33] Al-Sarawy A, Rashed IG, Hanna MA, et al. Removal of some 4-pyrazolone dyes from aqueous solutions by adsorption onto different types of carbon. Desalination. 2005;186(1–3):129–153.
[34] Rezaee A, Rangkooy H, Jonidi-jafari A, et al. High photocatalytic decomposition of the air pollutant formaldehyde using nano-ZnO on bone char. Environ Chem Lett. 2014;12:353–357.
[35] Rezaee A, Rangkooy H, Jonidi-jafari A, et al. Surface modification of bone char for removal of formaldehyde from air. Appl Surf Sci. 2013;286:235–239.
[36] Reynel-Avila HE, Mendoza-Castillo DI, Bonilla-Petriciolet A, et al. Assessment of naproxen adsorption on bone char in aqueous solutions using batch and fixed-bed processes. J Mol Liq. 2015;209:187–195.
[37] Reynel-Avila HE, Mendoza-Castillo DI, Bonilla-Petriciolet A, et al. Relevance of anionic dye properties on water decolorization performance using bone char: adsorption kinetics, isotherms and breakthrough curves. J Mol Liq. 2016;219:425–434.

[38] Nigri EM, Bhatnagar A, Rocha SDF. Thermal regeneration process of bone char used in the fluoride removal from aqueous solution. J Clean Prod. 2017;142:3558–3570.
[39] Nigri EM, Cechine MAP, Mayer DA, et al. Cow bones char as a green sorbent for fluorides removal from aqueous solutions: batch and fixed-bed studies. Environ Sci Pollut Res. 2016. DOI:10.1007/s11356-016-7816-5
[40] Aksu Z, Gönen F. Binary biosorption of phenol and chromium (VI) onto immobilized activated sludge in a packed bed: prediction of kinetic parameters and breakthrough curves. Sep Purif Technol. 2006;49:205–216.
[41] Nascimento RF, Lima ACA, Vidal CB, et al. Adsorção aspectos teóricos e aplicações ambientais [Adsorption: theoretical aspects and environmental applications]. Fortaleza, CE: Imprensa Universitária; Portuguese; 2014. p. 256.
[42] Reynolds TD, Richards PA. Unit operations and processes in environmental engineering. 2nd ed. Stamford: Cengage Learning; 1996. p. 798.
[43] ABNT – Associação Brasileira de Normas Técnicas [Brazilian Association of Technical Standards] [Internet]. ABNT NBR NM 27:2001 – Aggregates – Reducing field samples to laboratory testing size; 2001 [cited 2015 Oct]. Available from: https://www.abntcatalogo.com.br/norma.aspx?ID=306
[44] APHA – American Public Health Association. Standard methods for the examination of water and wastewater. 22nd ed. Washington; 2012.
[45] Gupta VK, Srivastava SK, Mohan D. Equilibrium uptake, sorption dynamics, process optimization, and column operations for the removal and recovery of malachite green from wastewater using activated carbon and activated slag. Ind Eng Chem Res. 1997;36:2207–2218.
[46] Bertoni FA, Medeot AC, González JC, et al. Application of green seaweed biomass for Mo^{VI} sorption from contaminated waters: kinetic, thermodynamic and continuous sorption studies. J Colloid Interface Sci. 2015;446:122–132.
[47] Hamdaoui O. Removal of copper (II) from aqueous phase by Purolite C100-MB cation exchange resin in fixed bed columns: modeling. J Hazard Mater. 2009;161:737–746.
[48] Lezehari M, Baudu M, Bouras O, et al. Fixed-bed column studies of pentachlorophenol removal by use of alginate-encapsulated pillared clay microbeads. J Colloid Interface Sci. 2012;379(1):101–106.
[49] Albadarin AB, Mangwandi C, Al-Muhtaseb AH, et al. Kinetic and thermodynamics of chromium ions adsorption onto low-cost dolomite adsorbent. Chem Eng J. 2012;179:193–202.
[50] Hamdaoui O. Batch study of liquid-phase adsorption of methylene blue using cedar sawdust and crushed brick. J Hazard Mater. 2006;135(1–3):264–273.
[51] Mesquita PL, Cruz MAP, Souza CR, et al. Removal of refractory organics from saline concentrate produced by electrodialysis in petroleum industry using bone char. 12th International Conference on the Fundamentals of Adsorption, FOA; 2016 29 May–3 June; Friedrichshafen/Lake Constance, Germany; 2016.
[52] Thommes M, Kaneko K, Neimark A, et al. Physisorption of gases, with special reference to the evaluation of surface area and pore size distribution (IUPAC Technical Report). Pure Appl Chem. 2015;87(9–10):1051–1069.
[53] McCabe WL, Smith JC, Harriott P. Unit operations of chemical engineering. 7th ed. New York, NY: McGraw Hill Education; 2005. p.1168.
[54] Han R, Zou W, Li H, et al. Copper (II) and lead (II) removal from aqueous solution in fixed-bed columns by manganese oxide coated zeolite. J Hazard Mater. 2006;137:934–942.
[55] Liu J, Huang X, Liu J, et al. Adsorption of arsenic (V) on bone char: batch, column and modeling studies. Environ Earth Sci. 2014;72:2082–2090.
[56] Song J, Zou W, Bian Y, et al. Adsorption characteristics of methylene blue by peanut husk in batch and column modes. Desalination. 2011;265:119–125.
[57] Thomas HC. Heterogeneous ion exchange in a flowing system. J Am Chem Soc. 1944;66:1664–1666.
[58] Delgado JMPQ. A critical review of dispersion in packed beds. Heat Mass Transfer. 2006;42:279–310.
[59] Celenza GJ. Industrial waste treatment engineering: specialized treatment systems, volume III. New York, NY: Taylor Francis Inc; 2001.
[60] Wolborska A. Adsorption on activated carbon of p-nitrophenol from aqueous solution. Water Res. 1989;23(1):85–91.
[61] Wolborska A, Pustelnik P. A simplified method for determination of break-through time of an adsorbent layer. Water Res. 1996;30(11):2643–2650.
[62] Bohart GS, Adams EQ. Some aspects of the behavior of charcoal with respect to chlorine. J Chem Soc. 1920;42:523–544.
[63] Singh S, Srivastava VC, Mall ID. Fixed- bed study for adsorptive removal of furfural by activated carbon. Colloid Surface A Physicochem Eng Asp. 2009;332:50–56.